Pergamon

PII: S0191-8141(97)00040-0

Journal of Structural Geology, Vol. 19, No. 9, pp. 1137 to 1148, 1997
© 1997 Elsevier Science Ltd
All rights reserved. Printed in Great Britain
0191-8141/97 $17.00 + 0.00

Deformation of garnets in a low-grade shear zone

ANTONIO AZOR,* J. FERNANDO SIMANCAS, INMACULADA EXPOSITO, FRANCISCO GONZALEZ LODEIRO and DAVID J. MARTINEZ POYATOS

Departamento de Geodinámica, Universidad de Granada, Campus de Fuentenueva, E-18002 Granada, Spain

(*Received* 18 *November* 1996; *accepted in revised form* 7 *May* 1997)

Abstract—Elongated shapes of garnets in high-grade metamorphic rocks have been explained as a result of plastic crystal flow or anisotropic growth. In the case of low- to medium-grade metamorphic rocks, a satisfactory explanation has not been proposed yet for elongated garnets. We have studied elongated garnets grown under low-grade metamorphic conditions in a shear zone with a composite planar-linear fabric. Garnet shapes in three dimensions define oblate ellipsoids. Drawing on evidence from compositional X-ray maps, it can be deduced that growth zoning is truncated along the long borders of grains, whereas subcircular garnets show non-truncated concentric growth zoning. This fact shows that selective dissolution along planes parallel to the foliation and the *C* surfaces can be claimed to be the main mechanism responsible for the deformation of the garnets under examination here. More specifically, dislocation-enhanced dissolution, which occurs at low temperatures and low dislocation mobility, is arguably the mechanism responsible for partially dissolving the garnet grains. Selective dissolution is expected to yield plane-strain oblate ellipsoids (i.e. with a volume loss) as measured in the elongated garnets. However, the rock as a whole has been deformed by plastic flow in a simple-shear regime, as shown by the existence of numerous shear criteria and the strain calculations performed. © 1997 Elsevier Science Ltd.

INTRODUCTION

Garnet is a mineral commonly found in metapelitic rocks of varying metamorphic conditions. This mineral usually forms idiomorphic or equidimensional crystals irrespective of the deformation and temperature undergone by the rock. In foliated metamorphic rocks, garnet appears generally as subcircular grains (subspherical in three dimensions) with different temporal relationships regarding foliation development. Therefore, it can be claimed that this mineral is quite unlikely to be deformed in a range of temperatures from low to high grade.

Despite the widespread subcircular shapes, some examples of elongated garnets have been reported. Ji and Martignole (1994, 1996) have described strongly non-equidimensional garnets in high-grade metamorphic rocks, concluding that garnet can be ductilely deformed at very high temperatures ($\geq$900°C). These authors have proposed that at such elevated temperatures garnet becomes weaker than quartz and feldspar giving way, as a consequence of ductile deformation by means of dislocation slip and recovery, to very elongated grains (but see the discussion by Den Brok and Kruhl, 1996). Another example of very elongated garnets was described by Blackburn and Dennen (1968) in high-grade rocks made up of biotite, sillimanite, K-feldspar and cordierite. In this case, garnets in adjacent quartz–feldspar mm-scale layers are equidimensional and smaller than those included in more pelitic domains. These data led Blackburn and Dennen (1968) to conclude that different rates of diffusion along and across foliation provoked anisotropic growth of garnet. A similar explanation of anisotropic growth of garnets was claimed by Gresens (1966). More scarce still are the reports on elongated garnets at medium- to low-grade metamorphic conditions (e.g. Dalziel and Bailey, 1968; Ross, 1973). In these examples, the existence of moderately elongated garnets (oblate ellipsoids in three dimensions) in low-grade mylonites has been attested.

Anisotropic growth (including pseudomorphism) and ductile deformation can be responsible for the development of non-equidimensional garnets; the latter can take place by dislocation slip–recovery and selective dissolution. In order to be able to discriminate between these different mechanisms, further studies on the rheological properties, microstructures, shape, textural relationships and chemical zoning of the garnets need to be undertaken. In this paper we are concerned with the description of ellipsoidal garnets in a metapelitic rock from a low-grade shear zone. We have examined the shape of the garnets in three dimensions, as well as their chemical zoning, in order to decipher whether their forms are due to ductile deformation or anisotropic growth. The data obtained point to deformation by selective dissolution as the main cause of the elongated shapes of the garnets studied.

GEOLOGICAL SETTING

The sample studied belongs to the upper part of a unit (Central Unit; Azor *et al.*, 1994) located between the Central Iberian and the Ossa–Morena Zones in the Southwestern Iberian Massif (Fig. 1). The Central Unit is made up of metasediments, orthogneisses and amphibolites, organized in a sequence in which orthogneisses

*Author to whom correspondence should be addressed.

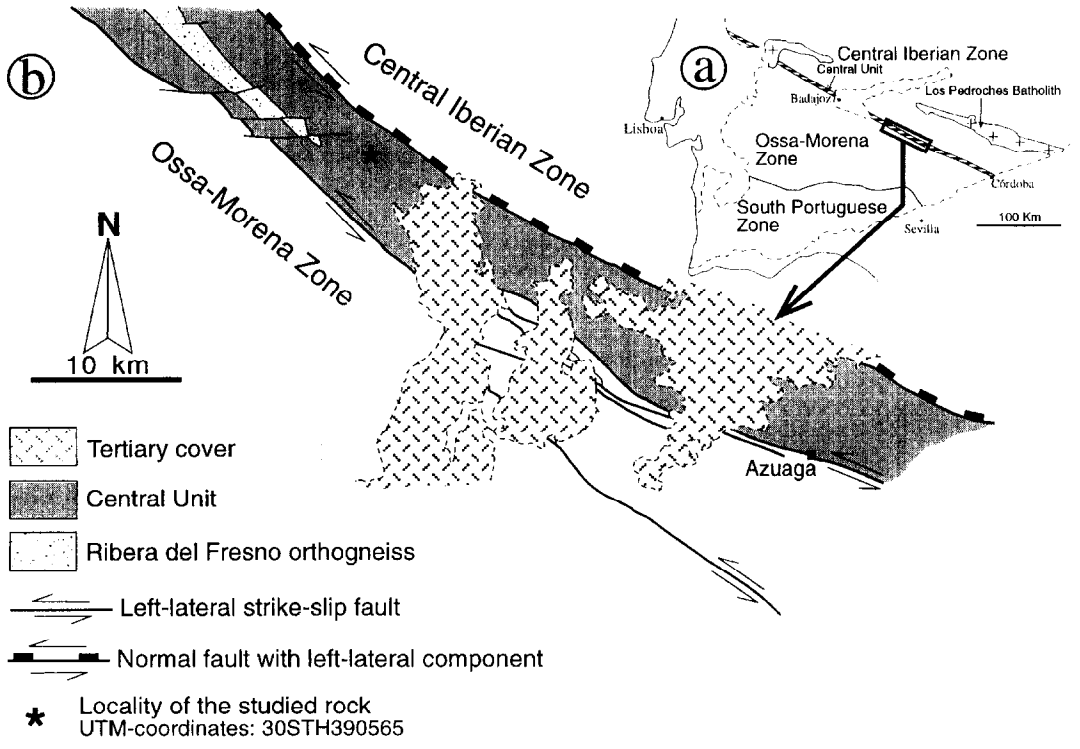

Fig. 1. (a) Geological sketch of the southwestern Iberian Massif showing the location of the area represented in (b) (rectangle). (b) Schematic geological map of the boundary between the Central Iberian and Ossa–Morena Zones in which the Central Unit is differentiated. The location and UTM coordinates of the rock studied are indicated.

and amphibolites appear in the lower part and metasediments in the upper part.

The Central Unit as a whole is affected by a ductile left-lateral shearing with an extensional component that provokes its exhumation (Azor *et al.*, 1994). This shearing generated a strongly developed composite planar and linear fabric which can be recognized throughout the unit. The metamorphic evolution of this unit is characterized by an initial high-pressure–high-temperature event ($P \geq 15$ kbar and $T \approx 650°C$) preserved as eclogite assemblages in garnet-bearing amphibolites (Abalos *et al.*, 1991) of the lower part. After this initial metamorphism, the lower part of the unit underwent an almost isothermal decompression first to amphibolite facies and then to greenschist facies (Azor *et al.*, 1994). The upper part of the unit recorded a similarly shaped *P–T* path, but peak pressure was lower (≤ 10 kbar) and temperature did not exceed 500–550°C (Azor, 1994).

Available radiometric datings have yielded Upper Silurian–Lower Devonian ages for the high-pressure–high-temperature metamorphism (Schäfer *et al.*, 1991) and Upper Devonian–Lower Carboniferous ages for the medium- and low-grade metamorphism (Quesada and Dallmeyer, 1994).

PETROGRAPHIC DESCRIPTION

The rock studied is a fine–medium-grained muscovite-bearing schist interbedded with quartzites and minor orthogneisses, located in the upper part of the Central Unit (Fig. 1b). This schist is made up of quartz, muscovite, garnet and minor biotite. It contains tourmaline, apatite and ilmenite as accessory phases. Petrographic observations under the microscope reveal a textural equilibrium between the different phases. Kyanite has been cited in the metapelites of the upper part of the Central Unit (Abalos *et al.*, 1991), although it has not been observed in the samples collected for the present study.

The rock concerned is an *S–C* mylonite (Fig. 2a & b) with the *S* surfaces marked by muscovite and recrystallized quartz ribbons. The stretching lineation is defined by quartz ribbons and pressure shadows in garnet.

Fig. 2. Photomicrographs of the studied rock in the *XZ* section. Sense of shearing is top-to-right in all microphotographs (left-lateral in map view, but right-lateral in the photographs). (a) & (b) General microscopic view of the garnet-bearing mica-schist where *S–C* structures, mica-fishes and elongated garnets can be observed. (c) Subelliptical elongated garnet with the long axis parallel to the *S* surfaces. (d) Subrectangular garnet grain with the long axis parallel to a *C* surface. Note quartz-inclusions defining an internal foliation oblique to the external one. (e) & (f) Asymmetric rounded pulled-out corners in elongated garnet grains. (g) Drop morphology in a very elongated garnet grain parallel to the *S* surfaces. (h) Very elongated garnet grain with bone morphology. Note the presence of an extensional crack filled with tourmaline in the central part of the garnet.

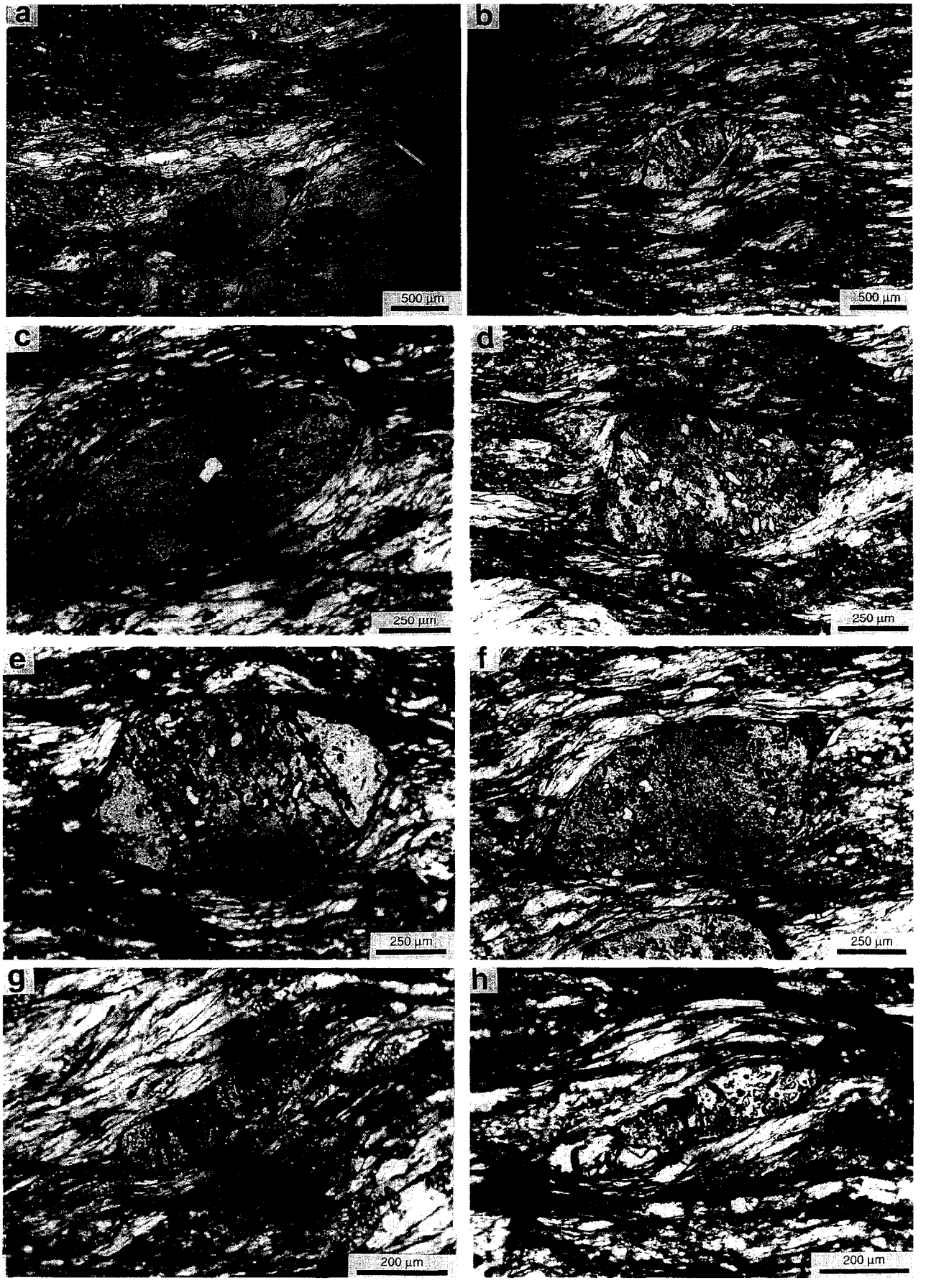
a
500 µm
b
500 µm
c
250 µm
d
250 µm
e
250 µm
f
250 µm
g
200 µm
h
200 µm

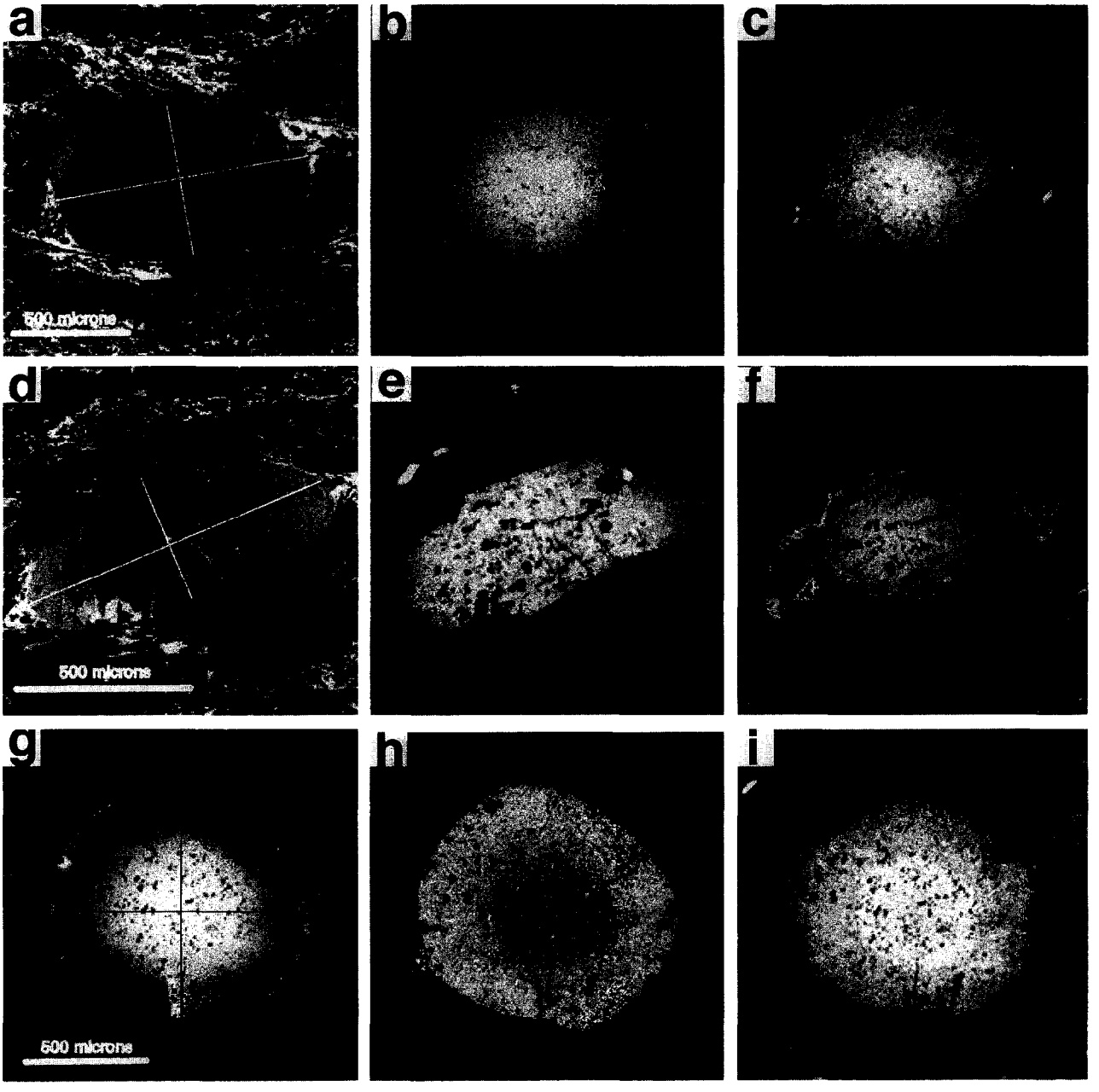

Fig. 3. X-ray maps of three garnets in the *XZ* section. For each garnet three images corresponding to three elements are shown. Contents of each element vary from clear coloured areas (maximum contents) to dark coloured ones (minimum contents). Actual contents of the different end-members (almandine, pyrope, spessartine and grossular + andradite) are shown in Fig. 6. (a)–(c) Moderately elongated garnet (Grt-1 in Fig. 6). (a) Mg X-ray map; the two perpendicular white lines locate the long- and short-axis profiles of this garnet in Fig. 6. (b) & (c) Mn and Ca X-ray maps; note truncation of Mn and Ca zoning along the long border of the grain. (d)–(f) Strongly elongated garnet (Grt-2 in Fig. 6). (d) Mg X-ray map; the two perpendicular white lines locate the long- and short-axis profiles of this garnet in Fig. 6. (e) & (f) Ca and Mn X-ray maps; note truncation of Ca zoning along the long border. (g)–(i) Subcircular garnet (Grt-3 in Fig. 6). (g) Mn X-ray map; the two perpendicular black lines locate E–W and N–S profiles of this garnet in Fig. 6. (h) & (i) Fe and Ca X-ray maps; note the concentric patterns of zoning in the three images.

Numerous shear criteria are visible in hand specimen and under the microscope indicating a left-lateral (i.e. top-to-the-NW) sense of movement. The most abundant shear criteria are *S*–*C* structures, which are usually accompanied by *C*′ surfaces, mica-fishes, dynamically recrystallized quartz grains oblique to the foliation and asymmetric microfolds. *C* and *C*′ surfaces are sometimes exclusively defined by a strong deflection of the *S* surfaces but, more often than not, they are discontinuities marked by oxide minerals and tiny platelets of muscovite, biotite and/or oxy-chlorite that cut the deflected *S* surfaces. These relationships are interpreted as being indicative of a relatively later development of the *C* and *C*′ surfaces in comparison to the *S* surfaces (Lister and Snoke, 1984). These observations, together with the fact that the Central Unit was exhumed during the shearing, suggest

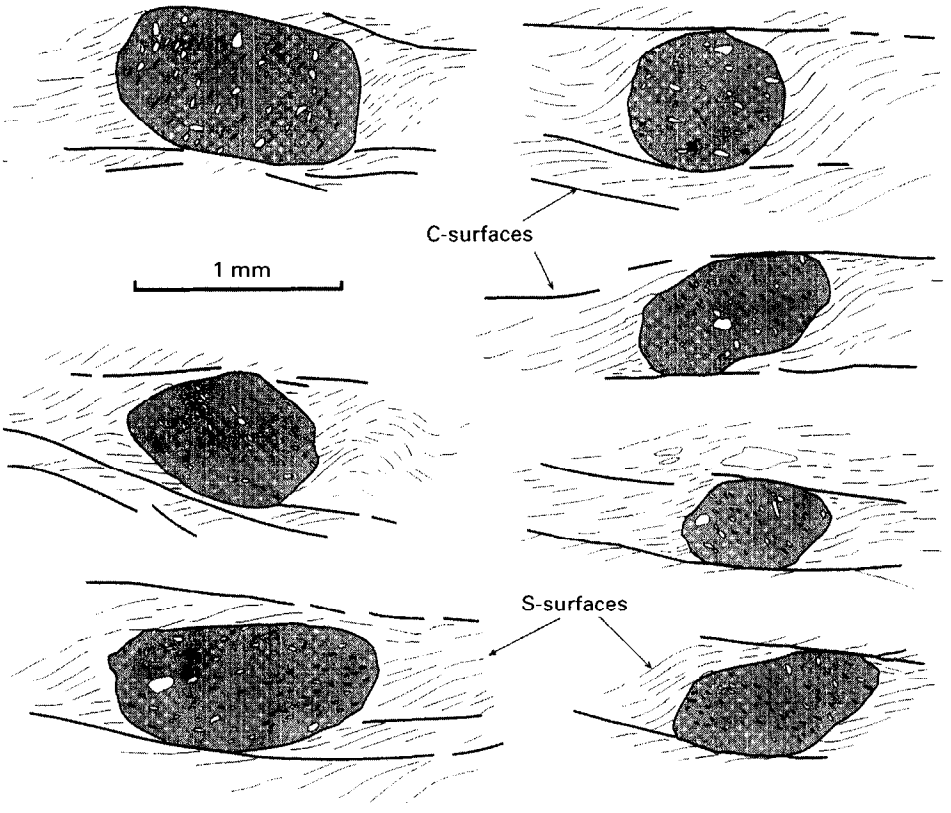

Fig. 4. Relationships between external and internal foliation in some garnets. Inclusions defining internal foliation are mainly made up of quartz (white pattern) and ilmenite (black pattern). The external foliation is marked by muscovite.

that the late stages of the shearing took place under retrograde conditions; i.e. at decreasing temperatures.

Garnet generally appears as elongated grains ranging in size from 0.2 to 1.2 mm (Figs 2 & 3). Inclusions in garnets are made up of quartz and ilmenite, which define in some cases an internal foliation more or less oblique with respect to the external foliation (Figs 2d & 4). The maximum angles between internal and external foliation are 80–90° measured in the sense of apparent rotation. Inclusion patterns suggest that garnet grew synchronously with at least a part of foliation development; i.e. the initial stages of the shearing. Pressure shadows in garnet show asymmetric patterns indicating the sense of shearing. They are made up of quartz, muscovite, biotite and tourmaline; these same minerals also fill extensional cracks affecting the garnets (Fig. 2h).

SHAPE OF THE GARNETS

Measurements of the three-dimensional garnet shape in separated individual grains cannot be accurately performed due to their small grain size ($\leq$1.2 mm). Consequently, we have measured garnet ellipticity in three mutually perpendicular sections: the *XZ* section (i.e. parallel to the stretching lineation and perpendicular to the foliation), the *YZ* section (i.e. perpendicular to both foliation and stretching lineation) and the *XY* section (i.e. parallel to the foliation).

Garnets in the *XZ* section show variably elongated shapes parallel to the foliation (Fig. 2c, g & h & Fig. 3d) or, in some cases, to the *C* surfaces (Fig. 2d). Although the general shape of garnets is approximately elliptical, they often display interesting shape variations when looked at in more detail. One of their most striking features is the presence of rounded asymmetric pulled-out corners indicating the same sense of movement as any other shear criteria observed in this rock (Fig. 2b, d, e & f). Similar morphologies have been experimentally obtained by Ghosh and Ramberg (1976). A few very elongated grains show drop or bone morphologies (Fig. 2g & h), similar to the ones obtained by means of theoretical computations by Treagus *et al.* (1996). The long borders of grains are, more often than not, straight in such a way that the shape is rather rectangular than elliptical; the long borders of these rectangular grains frequently coincide with *C* surfaces (Fig. 2d & f).

Ellipticities in the *XZ* sections vary from 4.0 to 1.0, the mean value being 1.8 (Fig. 5). Maximum ellipticities correspond to small grains which generally display extensional cracks (Fig. 2h). However, from measurements in thin sections under the microscope, the

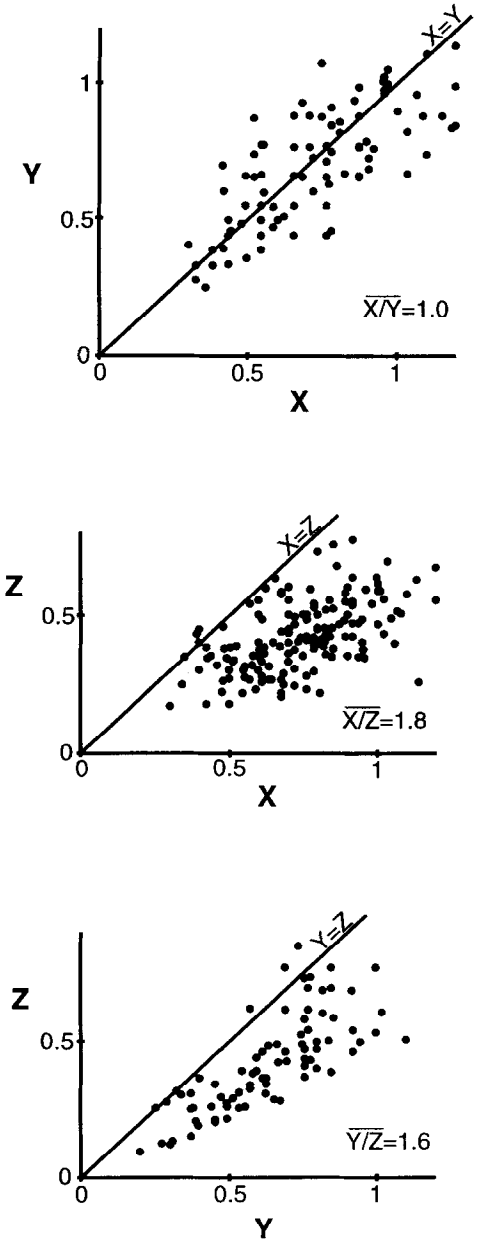

Fig. 5. *XY*, *XZ* and *YZ* diagrams for the garnets measured. The mean values are indicated.

maximum brittle extension is 35%. This brittle extension represents only a minor contribution to the total ellipticity of the grains.

The *YZ* sections show garnet ellipticities slightly lower than for the *XZ* sections (Fig. 5). Maximum ratios are about 2.7 and minimum ones about 1.0, the mean value being 1.6. In these sections, garnets do not have extensional cracks and pressure shadows are uncommon and poorly developed. Straight long borders can also be observed in the *YZ* sections, which, together with those observed in *XZ* sections, define planar surfaces perpendicular to the *Z* axes in some garnets.

The *XY* sections show more or less equidimensional garnets, with ellipticities ranging between 1.7 and 0.6 and the mean value being 1.0 (Fig. 5).

According to these data, the three-dimensional garnet shape can be considered, on average, as very oblate ellipsoids; in fact, they correspond to superellipsoids according to Lisle (1988). This oblate shape can also be directly observed in separated grains. The mean ellipticity values on each section can be adjusted to an average ellipsoid with axial ratios of $X/Y/Z = 1.1/1.0/0.6$.

CHEMISTRY OF THE GARNETS AND THERMOBAROMETRIC CONDITIONS

Garnet composition has been analysed with an electron microprobe CAMECA SX50 using the PAP correction. Analytical conditions were 20 kV accelerating voltage, 15 nA sample current and 15–40 s of counting time. Standards were synthetic oxides (Al_2O_3, Fe_2O_3, Cr_2O_3, $MnTiO_4$ and MgO), albite (Na), orthoclase (K) and wollastonite (Ca, Si). All elements were detected using the Kα ray.

The garnets analysed (see Table 1 and Fig. 6) are almandine-rich solid solutions (72–88 mol %) with subordinate pyrope (3.5–7.5 mol %), spessartine (2–10.5 mol %) and grossularite + andradite (2–15 mol %) contents. Fe^{3+} contents have been estimated, according to Droop (1987), to vary between 0 and 0.1 per formula unit on a basis of 12 oxygens and eight cations.

Zoning profiles from rim to rim through the core have been performed along two mutually perpendicular directions which coincide with the major and minor axes of the elongated garnets in the *XZ* sections. Most garnets are characterized by a decrease in spessartine and grossular + andradite, and an increase in almandine and pyrope, contents from core to rim (Fig. 6). Fe/Fe + Mg ratios slightly decrease from core to rim. These profiles (bearing in mind the garnet sizes and the biotite/garnet ratio) can be interpreted as growth zoning during prograde metamorphism; i.e. increasing temperature (Tracy, 1982; Loomis, 1983; Chakraborty and Ganguly, 1990). Such profiles are indicative of temperatures corresponding to low- or medium-grade metamorphism ($\leq$550–600°C), as at higher temperatures profiles become flat due to homogenization by diffusion or show retrograde zoning in the outer rim due to re-equilibration during the cooling history (e.g. Loomis *et al.*, 1985; Spear, 1991).

The *P–T* conditions undergone by the rock studied can be established with the aid of thermobarometers and petrogenetic grids. Peak metamorphic temperatures have been calculated using the garnet–muscovite geothermometer. The use of the garnet–biotite geothermometer is not recommended for this rock as biotite is volumetrically very scarce with respect to garnet, which may imply a lack of chemical equilibrium between both phases. Moreover, no good-quality biotite analyses were obtained due to its small grain size. Among the several calibrations of the garnet–muscovite geothermometer, the best results in our case were obtained with the one by

Table 1. Representative garnet and muscovite analyses

Sample	AA-4	AA-4	AA-4	AA-4	AA-4	AA-4	AA-4	AA-4
Mineral	Garnet	Garnet	Garnet	Garnet	Garnet	Garnet	Muscovite	Muscovite
Analysis	Grt-1 (core)	Grt-1 (rim)	Grt-3 (core)	Grt-3 (rim)	Grt-2 (core)	Grt-2 (rim)	Mus-384	Mus-472
SiO_2	37.03	36.56	36.28	36.89	36.81	36.74	46.83	46.36
TiO_2	0.13	0.07	0.18	0.10	0.12	0.09	0.58	0.41
Al_2O_3	20.96	20.92	20.84	21.08	20.82	21.05	35.05	36.34
Cr_2O_3	0.01	0.02	0.02	0.00	0.01	0.02	0.00	0.01
FeO	34.31	39.41	33.46	37.50	35.30	36.47	1.39	1.48
MgO	1.01	1.89	0.96	1.51	1.08	1.86	0.73	0.50
MnO	3.73	0.92	3.63	0.89	1.75	1.31	0.04	0.02
CaO	3.96	0.85	4.76	2.83	4.28	2.99	0.00	0.01
Na_2O	0.00	0.00	0.00	0.00	0.00	0.00	0.68	0.56
K_2O	0.00	0.00	0.00	0.00	0.00	0.00	10.11	9.69
Total	101.15	100.65	100.10	100.80	100.17	100.51	95.41	95.37
Structural formulae on a basis of eight cations and 12 oxygens for garnet, and 11 oxygens for muscovite								
Si	2.983	2.970	2.956	2.979	2.988	2.970	3.105	3.066
Ti	0.008	0.004	0.011	0.006	0.008	0.005	0.029	0.020
Al	1.990	2.003	2.001	2.006	1.992	2.006	2.739	2.833
Cr	0.000	0.002	0.001	0.000	0.001	0.001	0.000	0.001
Fe^{3+}	0.052	0.077	0.095	0.035	0.024	0.063		
Fe^{2+}	2.260	2.600	2.185	2.497	2.72	2.403		
Fe (Total)	2.311	2.677	2.280	2.532	2.386	2.466	0.077	0.082
Mg	0.122	0.229	0.117	0.182	0.131	0.244	0.072	0.049
Mn	0.255	0.063	0.251	0.061	0.120	0.090	0.002	0.001
Ca	0.342	0.074	0.415	0.245	0.373	0.259	0.000	0.000
Na	0.000	0.000	0.000	0.000	0.000	0.000	0.087	0.071
K	0.000	0.000	0.000	0.000	0.000	0.000	0.855	0.817
Pyrope	0.040	0.075	0.039	0.061	0.044	0.075		
Almandine	0.763	0.880	0.039	0.061	0.792	0.807		
Grossularite + andradite	0.113	0.024	0.140	0.082	0.124	0.087		
Spessartine	0.084	0.021	0.084	0.020	0.040	0.030		
Fe/Fe + Mg	0.950	0.921	0.949	0.932	0.948	0.915	0.761	0.624

Hynes and Forest (1988). Three different models for garnet solid solution have been considered: ideal solid solution and the models by Hodges and Spear (1982) and Ganguly and Saxena (1984). The three models have yielded similar temperatures. The temperatures obtained for garnet rims and matrix muscovites range between 420 and 530°C, most of them nevertheless being in the interval 490 ± 25°C. These temperatures are in accordance with the paragenesis of this rock. Garnet cores and matrix muscovites yield temperatures in the interval 390–520°C, most of the estimates being in the range 470 ± 25°C. These temperatures are, on average, between 20–60°C lower than rim temperatures. The calculated temperatures are in the range where diffusion in the garnet cannot make enough progress in order to erase growth zoning.

Peak pressure is difficult to estimate in this rock because the absence of aluminium silicate precludes the use of the garnet–Al_2SiO_5–plagioclase–quartz (GASP) geobarometer. A maximum pressure can be derived from the fact that rutile is not present, thus implying pressures lower than the reaction almandine + rutile = ilmenite + kyanite + quartz, i.e. of the order of 10 kbar (Bohlen *et al.*, 1983). Taking into account the estimated temperatures, a minimum pressure of about 5 kbar can be drawn from the fact that kyanite is the only aluminium silicate cited in the metapelitic rocks of the upper part of the Central Unit.

To sum up, peak *P–T* conditions of the rock studied are most likely to be in the interval 490 ± 25°C and 5–10 kbar.

ZONING MAPS OF GARNETS

The compositional study of garnets (zoning profiles and thermobarometric calculations) has revealed that garnet grew at increasing, although nevertheless moderate, temperatures. The question that arises now is whether the elongated shapes are due to anisotropic growth or ductile deformation. In this respect, compositional zoning maps of garnet could provide valuable information. A first estimate of the chemical zoning of garnets in two dimensions can be drawn from the fact that in the elongated garnets, long-axis profiles are more bell-shaped than short-axis ones (Fig. 6). However, subcircular garnets (i.e. those which apparently are undeformed) show similar shaped zoning profiles in two mutually perpendicular directions (Fig. 6). This fact seems to indicate that growth zoning is cut along the long borders of the elliptical garnets. To back up this statement, compositional X-ray maps of Fe, Mg, Mn and Ca were obtained with an electron microprobe. These maps effectively show that growth zoning in elongated garnets is cut along the long borders (Fig. 3a–f), i.e. those parallel to the foliation or the *C* surfaces; in the cores of

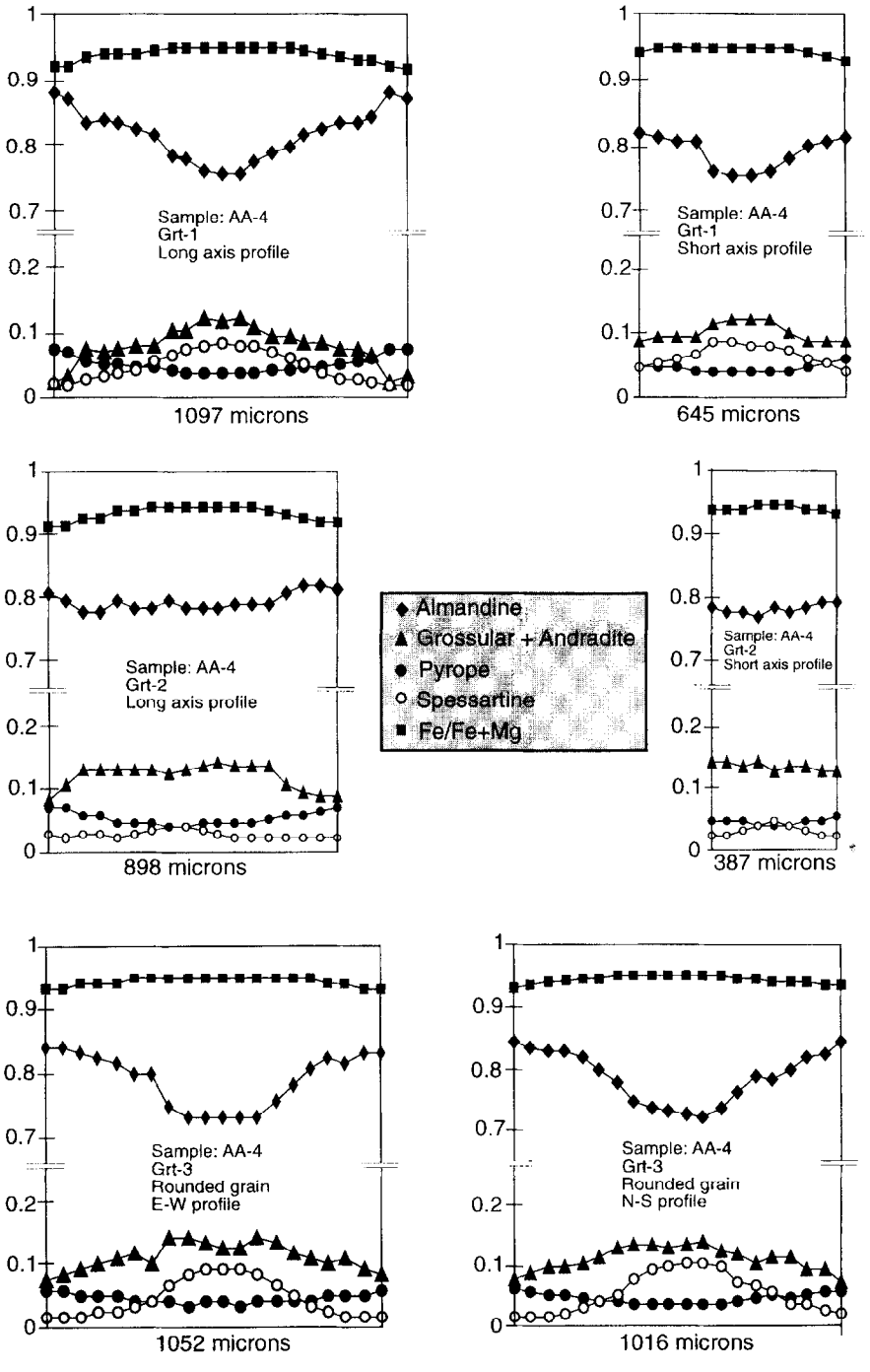

Fig. 6. Garnet zoning profiles from rim to rim through the core. Compare the profiles with the X-ray maps in Fig. 3.

these grains, a subcircular zoning still remains (Fig. 3c). By contrast, in subcircular garnets, growth zoning is concentric in the whole grain (Fig. 3g–i). These data enable us to conclude that elongated garnets have been partially dissolved after growth during the late stages of shearing. Consequently, the main cause of the ellipsoidal shape of the garnets seems to be ductile deformation by selective dissolution rather than anisotropic growth. The existence of some deposition at the end of the grains facing the extension direction, coeval with selective dissolution, cannot be completely discarded. The ends of the grain in Fig. 3(c) could be interpreted in this way. However, we think that the deposition lengthening of the grains represents only a very minor contribution, if any, in the shaping of the garnets. As zoning has been demonstrated to be prograde, i.e. displaying increasing

temperature to the rim of the garnets (Fig. 6), and there is textural evidence of retrogression during the late stages of the shearing, it can be plausibly concluded that even the rims of the garnets must have grown before their partial dissolution.

The history of the garnets in the rock investigated can be seen in terms of a two-stage process: (1) prograde syn-kinematic growth during the initial stages of the shearing; and (2) partial dissolution along surfaces parallel to the foliation or the *C* planes during the late stage of the shearing.

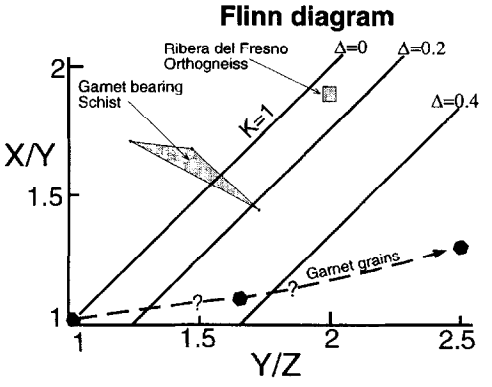

Fig. 7. Flinn diagram in which strain ellipsoids for garnets, whole rock and a neighbouring orthogneiss have been represented. Lines of plane strain for different values of volume loss (Δ) have been depicted.

STRAIN CALCULATIONS

Strain of the garnets

Having established that garnets have a truncated growth zoning, one can assume an initial subcircular shape (subspherical in three dimensions). Accordingly, the ellipsoidal shape of the garnets must reflect approximately their strain ellipsoid. The average shape ellipsoid calculated from the mean ellipticities in the three principal sections (see the section shape of the garnets) can be assimilated to the average strain ellipsoid of garnets ($X/Y/Z = 1.1/1.0/0.6$).

Also interesting (although somewhat less accurate) is the evaluation of the maximum strain ellipsoid recorded by garnets. From the data in Fig. 5, maximum X/Z and Y/Z ratios are 3.5–4.0 and 2.7, respectively. The maximum X/Y ratios are not obvious from the data obtained, as the influence of original shape variations in this almost non-strained section is very important (Lisle, 1977). However, given that the most elongated grains show brittle extension up to 35% along the X axis and no brittle extension along the Y axis, a maximum X/Y ratio of about 1.3 can be assumed. These three maximum ellipticities approximately fit to an ellipsoid $X/Y/Z = 1.3/1.0/0.4$. The minimum strain ellipsoid obviously corresponds to the subcircular grains and has approximately $X/Y/Z = 1.0/1.0/1.0$. The average, maximum and minimum strain ellipsoids plot in the oblate field of the Flinn diagram (Fig. 7). It is suggested that the line joining the projected points be interpreted as the strain path of the garnets.

Bulk strain

The garnet-bearing mica-schist studied has a strong planar-linear fabric, also developed throughout the Central Unit. At some outcrops, orthogneisses and amphibolites of this unit show a nearly linear fabric. Furthermore, in the XZ sections of the mica-schist there are abundant asymmetric structures indicating non-coaxial flow. Such asymmetric structures are not observed in the YZ sections. All this evidence strongly suggests simple shear as the main component of deformation (Berthé *et al.*, 1979a,b; Lister and Snoke, 1984; Gapais *et al.*, 1987) and, as a result, strain ellipsoids around $K = 1$ in the Flinn diagram should be expected for this rock. Despite the lack of good strain markers in the rock in question, some estimates of finite strain have been made on the basis of: (1) *S–C* angles; and (2) distances between the centres of garnet grains.

The use of *S–C* fabrics with a view to determining the magnitude of shear has been criticized in two different ways. On the one hand, if there is a flattening component in the deformation (subsimple-shear regime, Simpson and De Paor, 1993), the *S–C* angles would decrease, thus overestimating the magnitude of shear. We have no exact data on the vorticity in the rock studied and we will assume simple shear, as frequently done (e.g. Berthé *et al.*, 1979a; Burg *et al.*, 1981). On the other hand, it has been argued that the fabric tends to become steady state and therefore constant in orientation. Thus, in strongly deformed rocks, the *S–C* angles would underestimate the magnitude of shear (Williams *et al.*, 1994). In this respect, Lister and Snoke (1984) differentiated between type I (strain-sensitive) *S–C* fabrics and type II (strain-insensitive) *S–C* fabrics. A careful examination of the rocks studied shows that *S* surfaces are dominant as regards *C* surfaces, delineating continuous sigmoidal shapes (Fig. 2a & b). Moreover, in some quartz domains, a strain-insensitive foliation defined by small recrystallized quartz grains is oblique to the main foliation in the rock. From these observations, it can be concluded that the rock studied has a type I (largely strain-sensitive) *S–C* fabric. The *S–C* angles measured (θ') range between 33° and 22° with a mean value of 27° which, assuming simple shear ($\tan 2\theta' = -2/\gamma$, Ramsay and Huber, 1983, p. 27), corresponds to a mean shear value $\gamma = 1.46$ and an X/Z ratio of 3.8 (Fig. 7 & Table 2).

We have also tried to estimate the X/Z, Y/Z and X/Y axial ratios of the rock from the distances between the centres of garnets. A rigorous application of this method requires an initial anticlustered distribution of objects (Fry, 1979). Unfortunately the distribution of garnet grains shows domains of aggregates, which denotes that the initial distribution was not anticlustered. However,

Table 2. Summary of strain data for the whole rock

Rock	Method	Section	$\overline{X/Z}$	Y/Z	X/Y	γ	Data
Garnet-bearing schist	Distance between garnet centres	*XZ*, *YZ*, *XY*	3.6	2.5	1.7		287
Garnet-bearing schist	*S-C* angles	*XZ*	3.8			1.46	20
Neighbouring orthogeneiss	Distance between K-feldspar centres	*XZ*, *YZ*	3.9	2.1			138

the initial distribution of objects inside a given aggregate can be anticlustered, in which case an examination of such subareas can give information about strain. With these caveats in mind, we have measured the distances between centres only in obvious domains of aggregates. In *XZ* sections, from 125 measurements, the ratio between the mean distances of centres along the *X* (trace of the foliation) and *Z* axes is 3.6. This value is a little lower than the estimate made from *S–C* angles. In the same way, from 82 measurements in *YZ* sections, the estimated ratio is 2.5. In *XY* sections, from 89 measurements, the estimated ratio is 1.7 (Fig. 7 & Table 2). This result can only be taken as tentative as the ratios measured do not fit into a single ellipsoid. However, considering pairs of ratios and calculating the theoretical third one, three extreme ellipsoids can be obtained which define a triangular area in the Flinn diagram (Fig. 7). The baricentre of this triangle is close to $K=1$, thus lending some additional support to the assumption that the deformation of the rock is dominated by simple shear.

Strain estimates in an orthogneissic body (Ribera del Fresno orthogneiss, Fig. 1b) that intrudes the garnet-bearing mica-schists have also been performed. This orthogneiss is characterized by a striking type I (strain-sensitive) *S–C* fabric similar to that in the garnet-bearing mica-schists. Distances between centres of cm-scale K-feldspar grains along the *X*, *Y* and *Z* axes have been measured in *XZ* and *YZ* sections. From 103 measurements in *XZ* sections, we have obtained a ratio $X/Z=3.9$. From 35 measurements in *YZ* sections, the resulting Y/Z ratio is 2.1. The strain ellipsoid fitting these two strain ellipses has been represented in the Flinn diagram (Fig. 7) and is very close to $K=1$.

This result is once again compatible with the assumption of simple shear as the main component of the deformation in the rock studied.

Bulk strain vs garnet strain

The comparison between the strain ellipsoids of the elongated garnets and the whole rock shows that the main difference is the X/Y ratio (Fig. 7). For the rock the estimated X/Y ratio is consistent with simple shear, which implies stretching along the *X* axis and no stretching along *Y*. Conversely, for the garnets, X/Y ratios are around 1, except in grains affected by brittle extension with estimated maximum X/Y ratios of 1.3.

The fact that garnet deformation does not reflect the bulk deformation of the rock as a whole can be explained in terms of its greater rigidity that led to a predominant role of selective dissolution instead of crystalline plastic flow. Selective dissolution alone produces oblate plane-strain ellipsoids, thus implying volume loss. In this regard, considering the mean value of the X/Z ratio for garnet (1.8), the theoretical volume loss for an initial circular grain undergoing selective dissolution along *Z* is $\Delta \approx 0.4$ and, as shown in the Flinn diagram (Fig. 7), with such a volume loss, the average strain ellipsoid of garnets is a plane-strain one.

INTERPRETATION AND CONCLUSIONS

The main conclusions of the present study can be summarized as follows.

Garnets grew during low-grade metamorphic conditions ($T \approx 490 \pm 25$°C) in a shear zone responsible for the development of a penetrative planar-linear fabric.

Garnet shapes correspond to oblate ellipsoids. In *XZ* sections, garnets show an approximately elliptical shape. There are, however, some interesting features that must be emphasized, namely, the presence of asymmetric rounded pulled-out corners and straight long borders parallel to the *C* surfaces in *XZ* sections; straight long borders are also visible in *YZ* sections. Exceptionally, drop and bone morphologies are observed.

The garnets studied show compositional growth zonings indicative of crystallization at increasing temperatures. Compositional X-ray maps of the elongated garnets show that the growth zoning is truncated along the long borders of the grains. Conversely, subcircular garnets show non-truncated concentric growth zoning. This fact precludes anisotropic growth as a likely mechanism of formation for the elongated garnets studied, thus pointing to deformation as the main cause of their elongated shape.

The strain recorded by the garnets is variable but it is always projected into the field of very oblate ellipsoids. This strain can be interpreted as a plane strain if an important volume loss is assumed. However, the bulk strain suffered by the rock is close to $K=1$ and is thus very different to that of the garnets.

Truncation of the growth zoning in the elongated garnets indicates that these grains have undergone

selective dissolution along planes parallel to the foliation and the *C* surfaces of the rock. Consequently, selective dissolution can be invoked as the main mechanism responsible for the deformation of the garnets, which accords well with their plane-strain oblate ellipsoids. By contrast, the rock as a whole has been deformed by plastic flow in a simple-shear regime as evidenced by the existence of a planar-linear fabric and numerous asymmetric structures in the *XZ* sections.

The variably rotated inclusions in garnets, as well as the preservation of growth zoning, enable us to envisage a syn-kinematic blastesis at moderate but increasing temperature ($\leq$550°C) and/or pressure conditions ($\leq$10 kbar) affecting these rocks during the early stages of the shearing. In a later retrograde stage of the shearing, garnets were partially dissolved by selective dissolution, thus giving way to a truncation of the growth zoning. For garnets with average deformation, selective dissolution produced a volume loss of approximately 40%. The removed material, together with a fluid phase, was probably involved in reactions and generated the minerals now found in extensional cracks and pressure shadows (tourmaline, biotite, muscovite and quartz). There is no conclusive evidence that the removed material has been deposited at the ends of the grains facing the extension direction. Such a deposition appears to exist in the grain shown in Fig. 3(c). However, in the case of this grain, as in the other grains analysed, the compositional zoning is prograde, which means that the rim must have been formed before the late retrograde stages of shearing during which selective dissolution took place.

Selective dissolution is the main mechanism of deformation in the garnets studied. However, it is common for the garnets to have asymmetric pulled-out corners (Ghosh, 1993, figs 17.28c & 17.30; Treagus *et al.*, 1996), which suggests deformation by crystalline plastic flow as being a subordinate mechanism in the deformation of these garnets. In this regard, Meike (1990) has suggested that high dislocation densities in grains can promote their selective dissolution, in a different way to the most common mechanism of pressure solution (Rutter, 1983). Dislocation-enhanced dissolution occurs at low temperatures and, hence, low dislocation mobility. We claim that this is probably the main mechanism involved in the selective dissolution of the garnets studied. Exceptionally, grains with drop (Fig. 2g) or bone (Fig. 2h) morphologies (Treagus *et al.*, 1996) can be noticed, which point to an exceptional ductile behaviour coexisting with the generally rigid one characteristic of these garnets. However, at present, we are unable to provide a satisfactory account for this paradoxical and, therefore, puzzling coexistence.

Other studies of elongated garnets in mylonitic rocks have revealed three-dimensional shapes corresponding to very oblate ellipsoids (e.g. Dalziel and Bailey, 1968; Ross, 1973; Ji and Martignole, 1994), which are not the type of ellipsoid expected in rocks with strong planar-linear fabrics. In these cases it has been suggested that garnets were deformed by crystalline plastic flow, but, according to the misfit between measured (oblate) and expected ($K \approx 1$) ellipsoids in garnet, we tentatively suggest that selective dissolution has probably been underestimated, especially in those cases of low-grade metamorphic conditions.

Acknowledgements—We are very grateful to José Miguel Azañón for a critical reading of an early version of the manuscript. Francisco Gonzálvez García has helped us to translate our 'Spanglish' text into English. We thank Miguel Angel Hidalgo for technical assistance during the microprobe work. Many thanks are due to K. Brodie, C. Simpson and S. Treagus for detailed reviews of the manuscript. Financial support was given by the CICYT PB.93-1149-C03-01 Project.

REFERENCES

Abalos, B., Gil Ibarguchi, J. I. and Eguiluz, L. (1991) Cadomian subduction/collision and Variscan transpression in the Badajoz–Córdoba shear belt, southwest Spain. *Tectonophysics* **199**, 51–72.

Azor, A. (1994) Evolución tectonometamórfica del límite entre las Zonas Centroibérica y de Ossa–Morena (Cordillera Varisca, SO de España). Tesis Doctoral, Universidad de Granada.

Azor, A., González Lodeiro, F. and Simancas, J. F. (1994) Tectonic evolution of the Boundary between the Central Iberian and Ossa–Morena Zones (Variscan Belt, SW Spain). *Tectonics* **13**, 45–61.

Berthé, D., Choukroune, P. and Gapais, D. (1979) Orientations préférenticlles du quartz et orthogneissification progressive en régime cisaillant: L'exemple du cisaillement sud-armoricain. *Bulletin de Minéralogie* **102**, 265–272.

Berthé, D., Choukroune, P. and Jegouzo, P. (1979) Orthogneiss mylonite and non-coaxial deformation of granites: the example of the South Armorican Shear Zone. *Journal of Structural Geology* **1**, 31–42.

Blackburn, W. H. and Dennen, W. H. (1968) Flattened garnets in strongly foliated gneisses from the Grenville series of the Gananoque area, Ontario. *American Mineralogist* **53**, 1386–1393.

Bohlen, S. R., Wall, V. J. and Boettcher, A. L. (1983) Experimental investigations and geological applications of equilibria in the system FeO–TiO_2–Al_2O_3–SiO_2–H_2O. *American Mineralogist* **68**, 1049–1058.

Burg, J. P., Iglesias, M., Laurent, Ph., Matte, Ph. and Ribeiro, A. (1981) Variscan intracontinental deformation: The Coimbra–Córdoba Shear Zone (SW Iberian Peninsula). *Tectonophysics* **78**, 161–177.

Chakraborty, S. and Ganguly, J. (1990) Compositional zoning and cation diffusion in garnets. In *Diffusion, Atomic Ordering, and Mass Transport: Selected Problems in Geochemistry*, ed. J. Ganguly. *Advances in Physical Geochemistry* **10**, 120–175.

Dalziel, I. W. D. and Bailey, S. W. (1968) Deformed garnets in a mylonitic rock from the Grenville Front and their tectonic significance. *American Journal of Science* **266**, 542–562.

Den Brok, B. and Kruhl, J. H. (1996) Ductility of garnet as an indicator of extremely high temperature deformation: Discussion. *Journal of Structural Geology* **18**, 1369–1373.

Droop, G. T. R. (1987) A general equation for estimating Fe^{3+} concentrations in ferromagnesian silicates and oxides from microprobe analyses using stoichiometric criteria. *Mineralogical Magazine* **51**, 431–435.

Fry, N. (1979) Random point distributions and strain measurement in rocks. *Tectonophysics* **60**, 89–105.

Ganguly, J. and Saxena, S. K. (1984) Mixing properties of aluminosilicate garnets: constraints from natural and experimental data and applications for geothermobarometry. *American Mineralogist* **69**, 88–98.

Gapais, D., Balé, P., Choukroune, P., Cobbold, P. R., Mahjoub, Y. and Marquer, D. (1987) Bulk kinematics from shear zone patterns: some field examples. *Journal of Structural Geology* **9**, 635–646.

Ghosh, S. K. (1993) *Structural Geology. Fundamentals and Modern Developments*. Pergamon Press, Oxford.

Ghosh, S. K. and Ramberg, H. (1976) Reorientation of inclusions by combination of pure shear and simple shear. *Tectonophysics* **34**, 1–70.

Gresens, R. L. (1966) Dimensional and compositional control of garnet growth by mineralogical environment. *American Mineralogist* **51**, 524–528.

Hodges, K. V. and Spear, F. S. (1982) Geothermometry, geobarometry and the Al_2SiO_5 triple point at Mt. Moosilauke, New Hampshire. *American Mineralogist* **67**, 1118–1134.

Hynes, A. and Forest, R. C. (1988) Empirical garnet–muscovite geothermometry in low-grade metapelites, Selwyn Range (Canadian Rockies). *Journal of Metamorphic Geology* **6**, 297–309.

Ji, S. and Martignole, J. (1994) Ductility of garnet as an indicator of extremely high temperature deformation. *Journal of Structural Geology* **16**, 985–996.

Ji, S. and Martignole, J. (1996) Ductility of garnet as an indicator of extremely high temperature deformation: Reply. *Journal of Structural Geology* **18**, 1375–1379.

Lisle, R. J. (1977) Estimation of tectonic strain ratio from the mean shape of deformed elliptical markers. *Geologie en Mijnbouw* **56**, 140–144.

Lisle, R. J. (1988) The superellipsoidal form of coarse clastic sediment particles. *Mathematical Geology* **20**, 879–890.

Lister, G. S. and Snoke, A. W. (1984) S–C mylonites. *Journal of Structural Geology* **6**, 617–638.

Loomis, T. P. (1983) Compositional zoning of crystals: a record of growth and reaction history. In *Kinetics and Equilibrium in Mineral Reactions*, ed. S. K. Saxena. *Advances in Physical Geochemistry* **3**, 1–60.

Loomis, T. P., Ganguly, J. and Elphick, S. C. (1985) Experimental determination of cation diffusivities in aluminosilicate garnets. II. Multicomponent simulation and tracer diffusion coefficients. *Contributions to Mineralogy and Petrology* **90**, 45–51.

Meike, A. (1990) Dislocation enhanced selective dissolution: an examination of mechanical aspects using deformation mechanism maps. *Journal of Structural Geology* **12**, 785–794.

Quesada, C. and Dallmeyer, R. D. (1994) Tectonothermal evolution of the Badajoz–Córdoba shear zone (SW Iberia): characteristics and $^{40}Ar/^{39}Ar$ mineral age constraints. *Tectonophysics* **231**, 195 213.

Ramsay, J. G. and Huber, M. I. (1983) *The Techniques of Modern Structural Geology. Volume 1: Strain Analysis.* Academic Press, London.

Ross, J. V. (1973) Mylonitic rocks and flattened garnets in the southern Okanagan of British Columbia. *Canadian Journal of Earth Sciences* **10**, 1–17.

Rutter, E. H. (1983) Pressure solution in nature, theory and experiment. *Journal of the Geological Society of London* **140**, 725–740.

Schäfer, H. J., Gebauer, D. and Nagler, T. F. (1991) Evidence for Silurian eclogite and granulite facies metamorphism in the Badajoz–Córdoba Shear belt, SW Spain. *Terra Abstracts (Supplement 6 to Terra Nova)* **3**, 11.

Simpson, C. and De Paor, D. G. (1993) Strain and kinematic analysis in general shear zones. *Journal of Structural Geology* **15**, 1–20.

Spear, F. S. (1991) On the interpretation of peak metamorphic temperatures in light of garnet diffusion during cooling. *Journal of Metamorphic Geology* **9**, 379–388.

Tracy, R. J. (1982) Compositional zoning and inclusions in metamorphic minerals. In *Characterization of Metamorphism Through Mineral Equilibria*, ed. J. M. Ferry. *Reviews in Mineralogy* **10**, 355–397.

Treagus, S. H., Hudleston, P. J. and Lan, L. (1996) Non-ellipsoidal inclusions as geological strain markers and competence indicators. *Journal of Structural Geology* **18**, 1167–1172.

Williams, P. F., Goodwin, L. B. and Ralser, S. (1994) Ductile deformation processes. In *Continental Deformation*, ed. P. L. Hancock, pp. 1–27. Pergamon Press, Oxford.